Electronic Supplementary Material (ESI) for Inorganic Chemistry Frontiers.

Supporting Information for "Insulin fibrillation is controlled and modulated by specific zinc binding sites"

Shira Ben-Shushan[a,b] Yifat Miller[a,b,*]

[a] *Department of Chemistry, Ben-Gurion University of the Negev, P.O. Box 653, Be'er Sheva 84105, Israel*

[b] *Ilse Katz Institute for Nanoscale Science and Technology, Ben-Gurion University of the Negev, Beér-Sheva 84105, Israel*

Corresponding author:

*Yifat Miller: ymiller@bgu.ac.il

Table of Content

Methods

Conformational energies and population for Zn^{2+}-insulin fibril-like oligomers

To determine the stabilities and populations of the variant models of Zn^{2+}-insulin fibril-like octamers, the trajectories of the last 5 ns were first extracted from the explicit molecular dynamics simulations excluding water molecules. The solvation energies of all systems were calculated using the Generalized Born Method with Molecular Volume (GBMV).[1,2] In the GBMV calculations, the dielectric constant of water was set to 80.0. The hydrophobic solvent-accessible surface area (SASA) term factor was set to 0.00592 kcal/mol·Å2. Each variant was minimized using 1,000 cycles, and the conformation energy is evaluated by grid based GBMV. The minimization does not change the conformations of each variant, but only relaxed the local geometries due to thermal fluctuation which occurred during the molecular dynamics simulations. A total of 500 conformations for each of the examined models were used to construct the free energy landscape of the six Zn^{2+}-insulin fibril-like octamers (models M1-M6) and to evaluate the conformer probabilities by using Monte Carlo simulations. In the first step, one conformation of conformer i and one conformation of conformer j was randomly selected. Then, the Boltzmann factor was computed as e-(Ej-Ei)/kT, where Ei and Ej are the conformational energies evaluated using the GBMV calculations for conformations i and j, respectively, k is the Boltzmann constant and T is the absolute temperature (298 K used here). If the value of the Boltzmann factor was larger than the random number, then the move from conformation i to conformation j was allowed. After 1 million steps, the conformations 'visited' for each conformer were counted. Finally, the relative probability of model n was evaluated as Pn= Nn/Ntotal, where Pn is the population of model n, Nn is the total number of conformations visited for model n, and Ntotal is the total steps. The advantages of using Monte Carlo simulations to estimate conformer probability lie in their good numerical stability and the control that they allow of transition probabilities among several conformers. Using all six models of Zn^{2+}-insulin fibril-like octamers that were generated in molecular dynamics simulations, we estimated the overall stability and populations for each conformer based on the molecular dynamics simulations, with the energy landscape being computed with GBMV for these conformers.

Structural analysis

The structural stability of insulin fibril-like octamer – model N, and the six models of Zn^{2+}-insulin fibril-like octamers – models M1-M6, were measured by using several analyses. The convergences of the simulated models were analyzed by root mean square deviations. The fluctuations of each residue along the sequence of insulin for all studied models were calculated via root-mean square fluctuations (RMSFs). To estimate the secondary structure of each model, we used the database of secondary structure of protein (DSSP) method. This method was applied in aim to provide the percentage of the β-sheet structure and the α-helix for each residue along the molecular dynamics simulations. The RMSFs and the DSSP analyses were computed for the last 5 ns of the simulations for each model.

We monitored the change in the inter-sheet distances (Cα backbone - Cα backbone distances) between the β-sheet domains within the insulin fibril-like octamers. The insulin fibril-like structure consists of two β-sheets. These two β-sheets are arranged in a parallel manner. One of the β-sheet is in chain A, and the second parallel β-sheet is in chain B. Two distances were measured between Cα in chain A to Cα in chain B. The first distance D1 is between Leu16 of chain A and Leu15 of chain B and the second distance is between Cys20 of chain A and Cys19 of chain B. The averaged distances were calculated while excluding the distances values obtained from the monomers that are in the ends of each octamer for the last 5 ns of the simulations.

Finally, to estimate the binding of Zn^{2+} to the various binding sites, the distances between the metal ion and the specific residues (His and Glu) in each model along the molecular dynamics simulations were measured. The cut-off distances between Zn^{2+} ion to each amino acid were taken from the MESPEUS database of geometry of metal sites in protein.[3] Previously, we applied these measurements to investigate metal-residues distances in other systems.[4-8] The distances provide us insights into the conservation of the metal-binding sites.

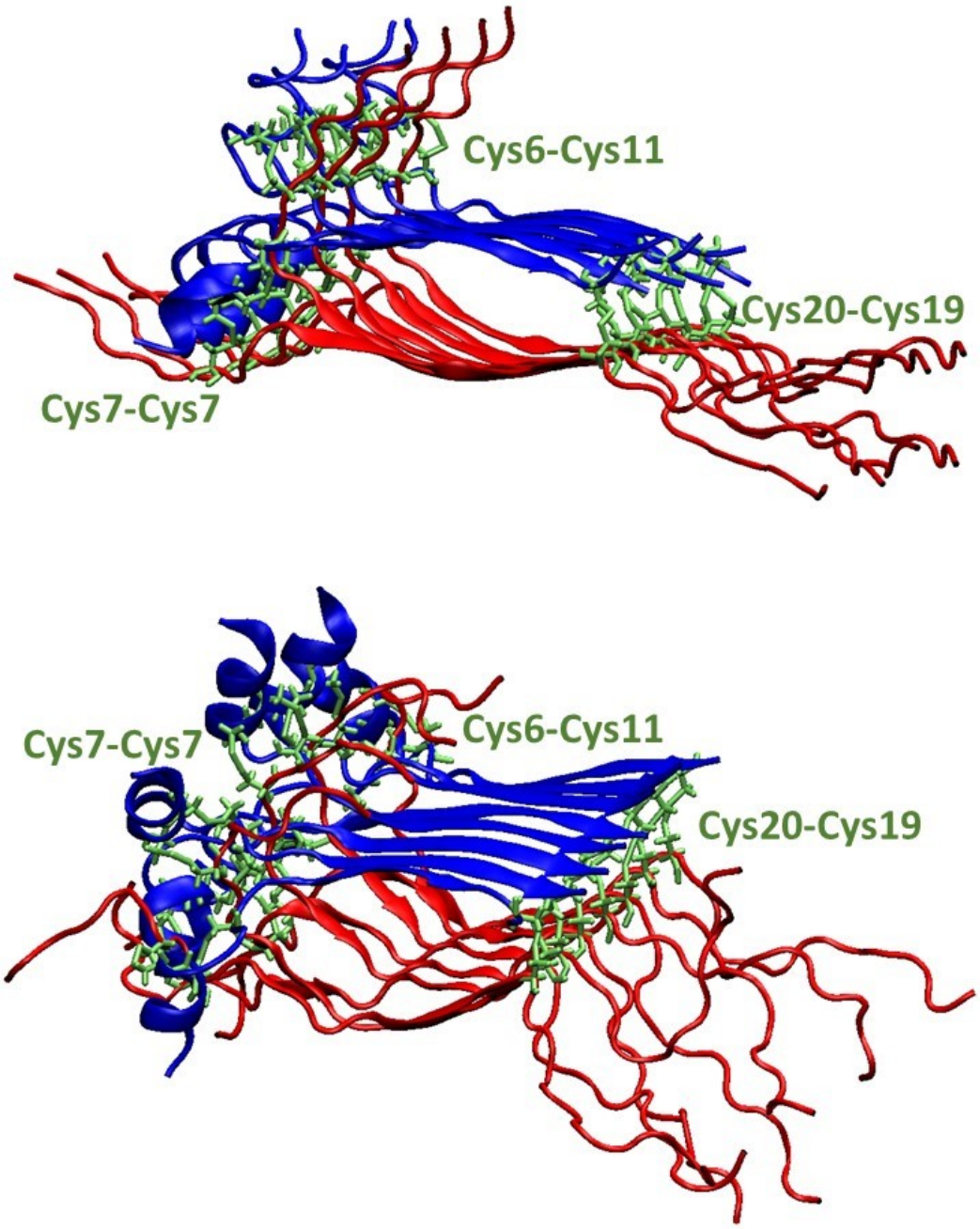

Figure S1: Initial (top) and simulated (bottom) insulin fibrillary model N. Insulin consists of chain A (color: blue), chain B (color: red), and three disulfide bonds (color: green): intra-chain linkage in chain A (Cys6-Cys11), and two inter-chain linkages (Cys7-Cys7 and Cys20-Cys19).

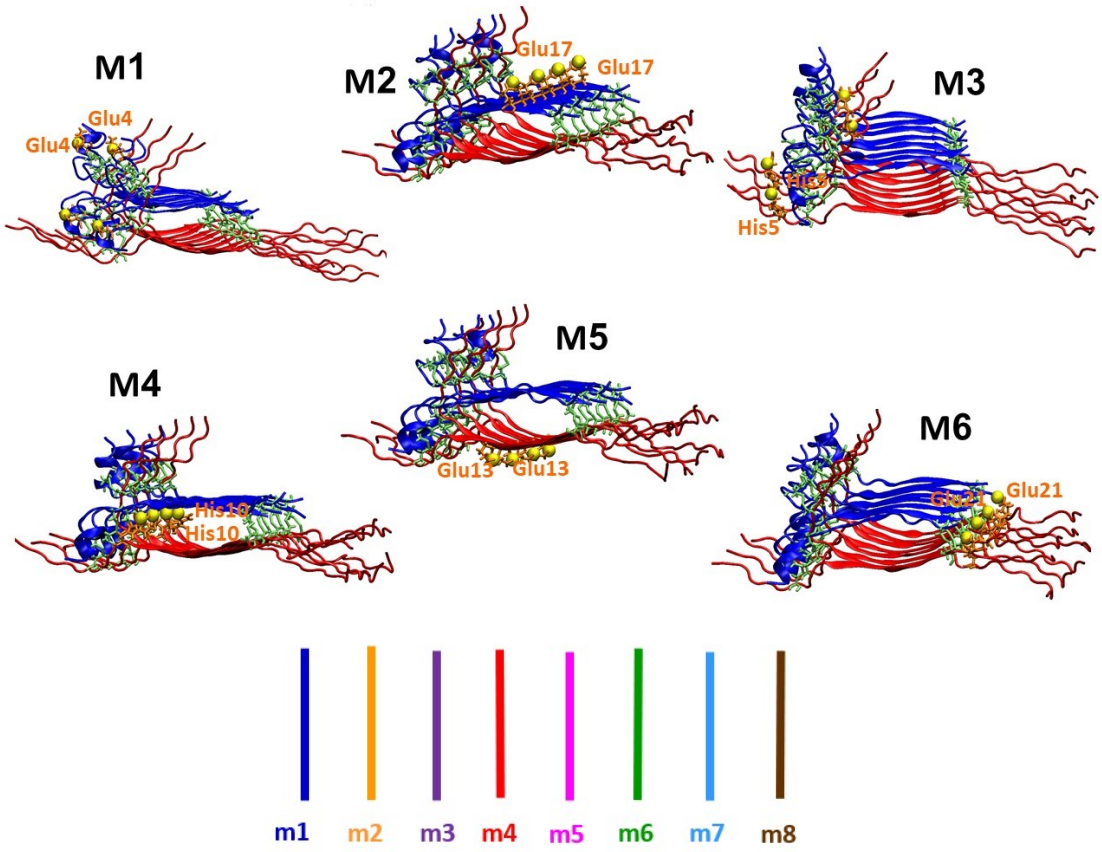

Figure S2: Initial insulin fibrillary structures that bind Zn^{2+} ions – models M1-M6. Insulin consists of chain A (color: blue), chain B (color: red), and three disulfide bonds (color: green): intra-chain linkage in chain A (Cys6-Cys11), and two inter-chain linkages (Cys7-Cys7 and Cys20-Cys19). In model M1: Zn^{2+} ions bind two Glu4 (chain A) in two following peptides. In model M2: Zn^{2+} ions bind two Glu17 (chain A) in two adjacent peptides. In model M3: Zn^{2+} ions bind two His5 (chain B) in two following peptides. In model M4: Zn^{2+} ions bind two His10 (chain B) in two adjacent peptides. In model M5: Zn^{2+} ions bind two Glu13 (chain B) in two adjacent peptides. In model M6: Zn^{2+} ions bind two Glu21 (chain B) in two adjacent peptides. Bottom: A scheme of the monomers within insulin fibril (left): monomer 1 (color: blue), monomer 2 (color: orange), monomer 3 (color: purple), monomer 4 (color: red), monomer 5 (color: pink), monomer 6 (color: green), monomer 7 (color: light blue), monomer 8 (color: brown).

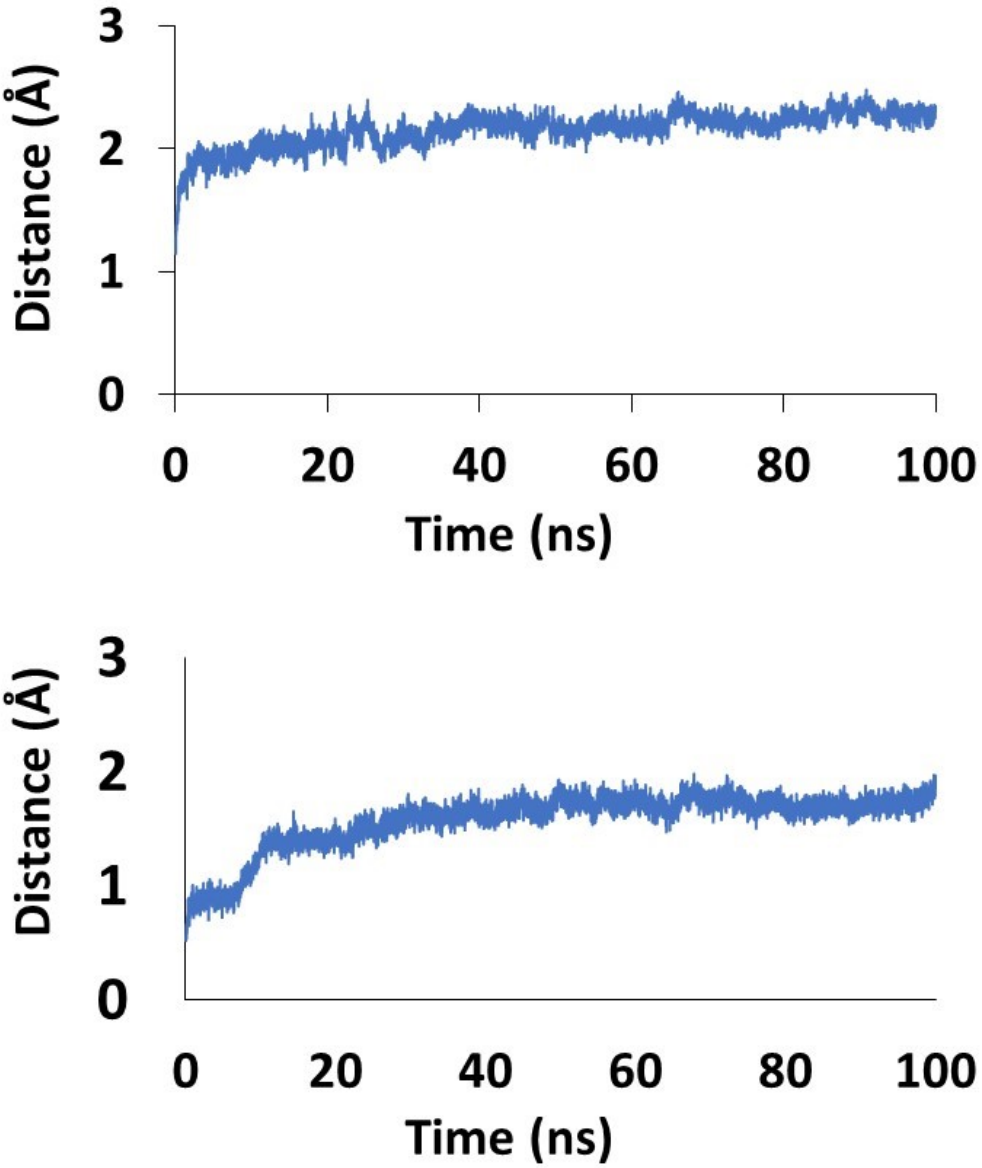

Figure S3: RMSDs of chain A (top) and insulin chain B, residues Ser9-Cys19 (bottom) of insulin fibril – model N.

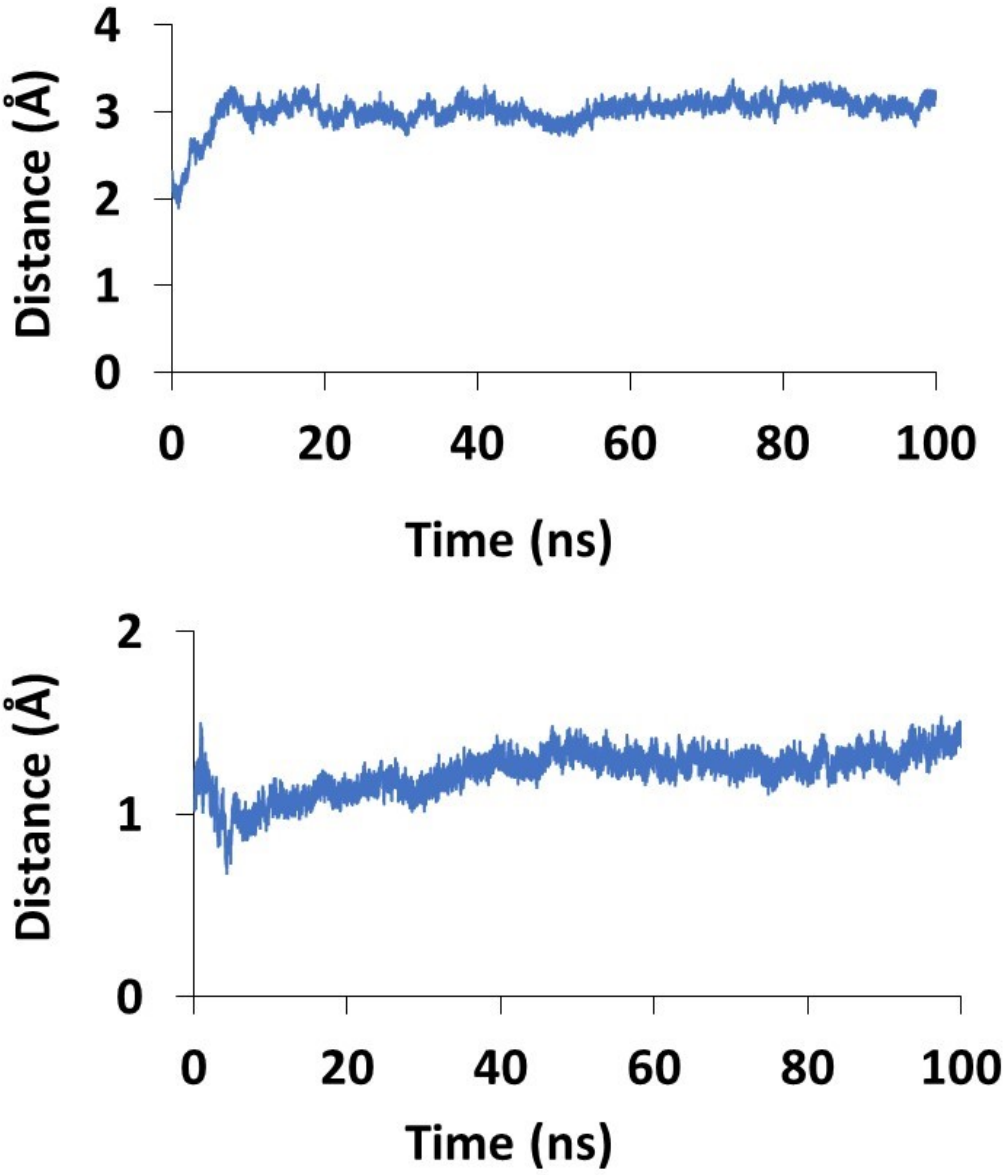

Figure S4: RMSDs of chain A (top) and insulin chain B, residues Ser9-Cys19 (bottom) of insulin fibril in which Zn^{2+} ions bind to chain A – model M1.

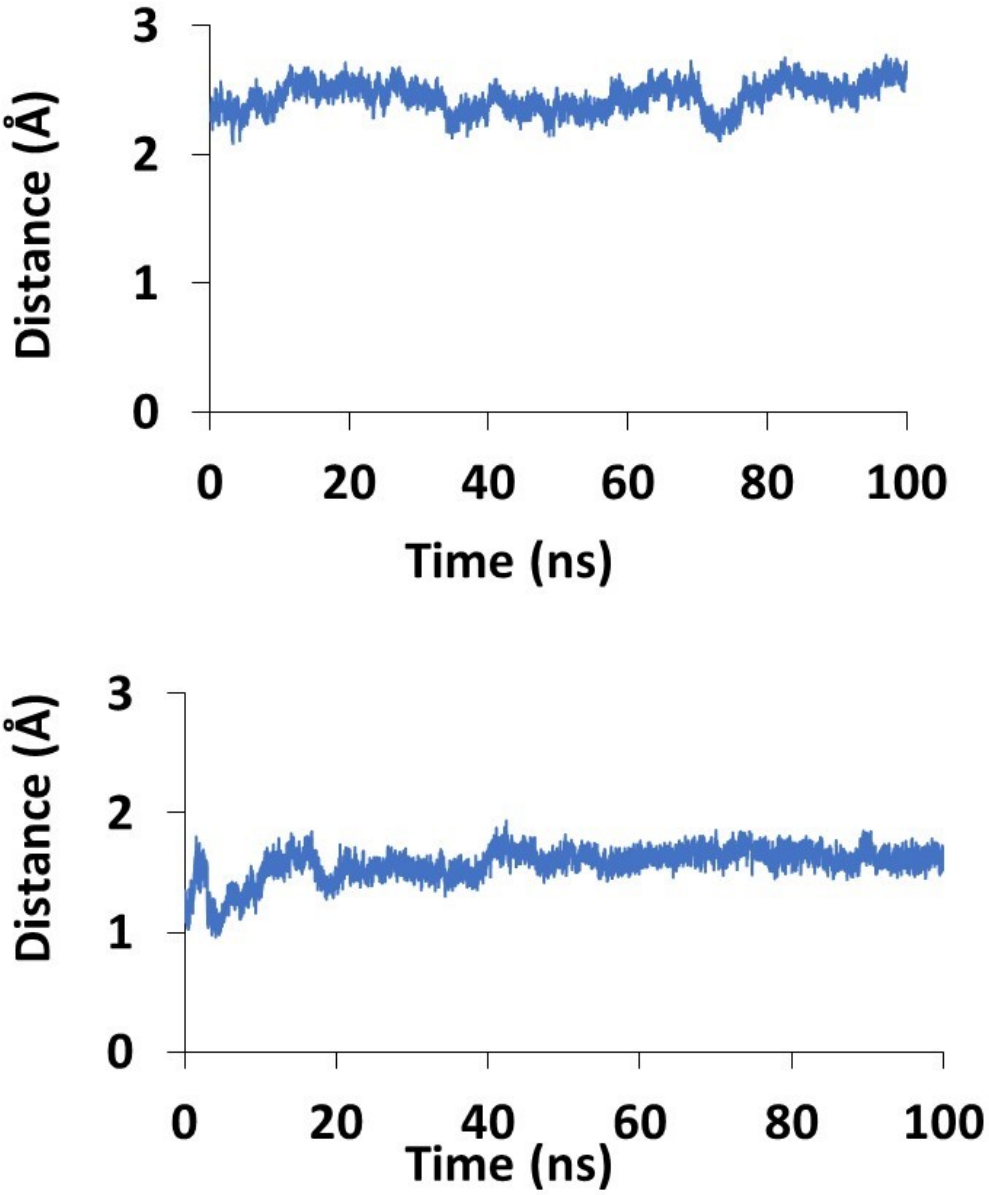

Figure S5: RMSDs of chain A (top) and insulin chain B, residues Ser9-Cys19 (bottom) of insulin fibril in which Zn^{2+} ions bind to chain A – model M2.

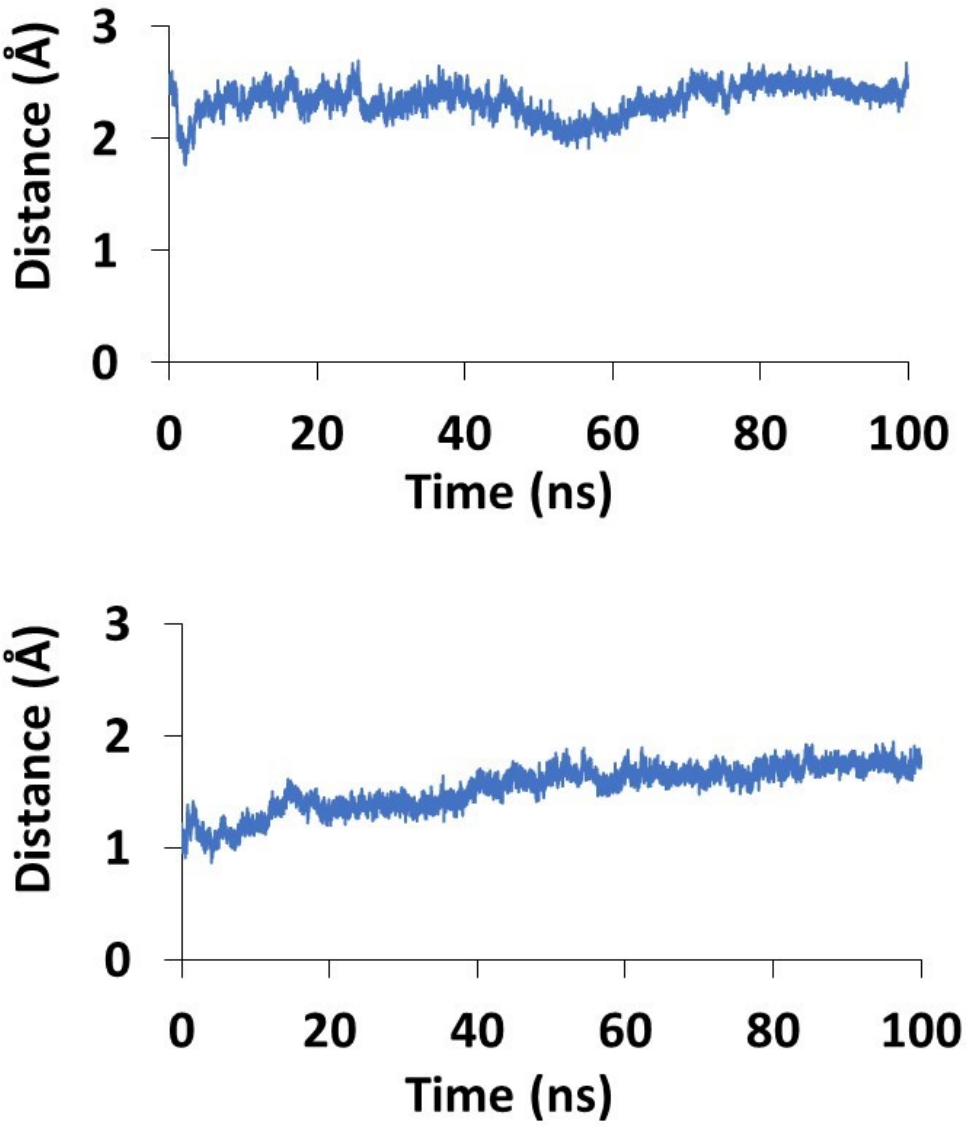

Figure S6: RMSDs of chain A (top) and insulin chain B, residues Ser9-Cys19 (bottom) of insulin fibril in which Zn^{2+} ions bind to chain B – model M3.

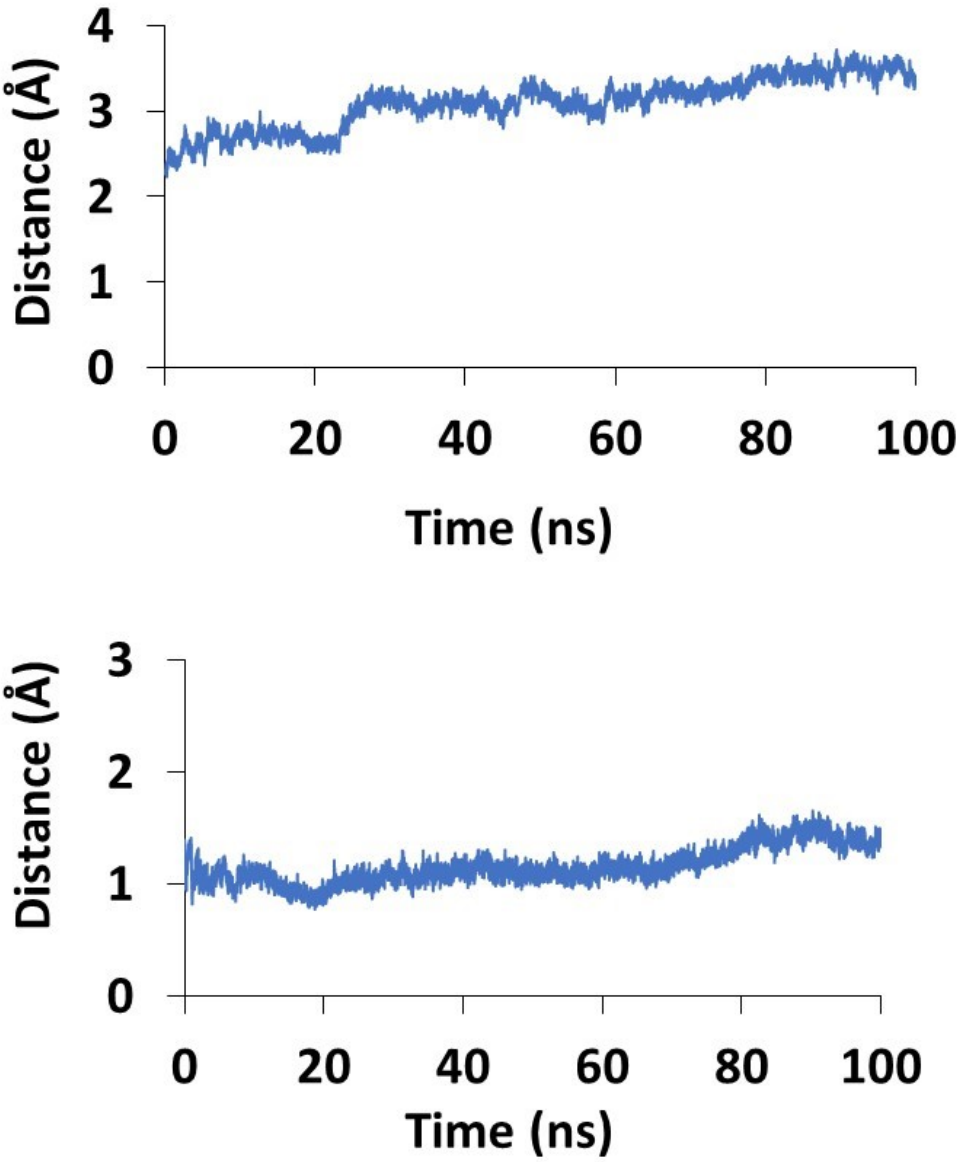

Figure S7: RMSDs of chain A (top) and insulin chain B, residues Ser9-Cys19 (bottom) of insulin fibril in which Zn^{2+} ions bind to chain B – model M4.

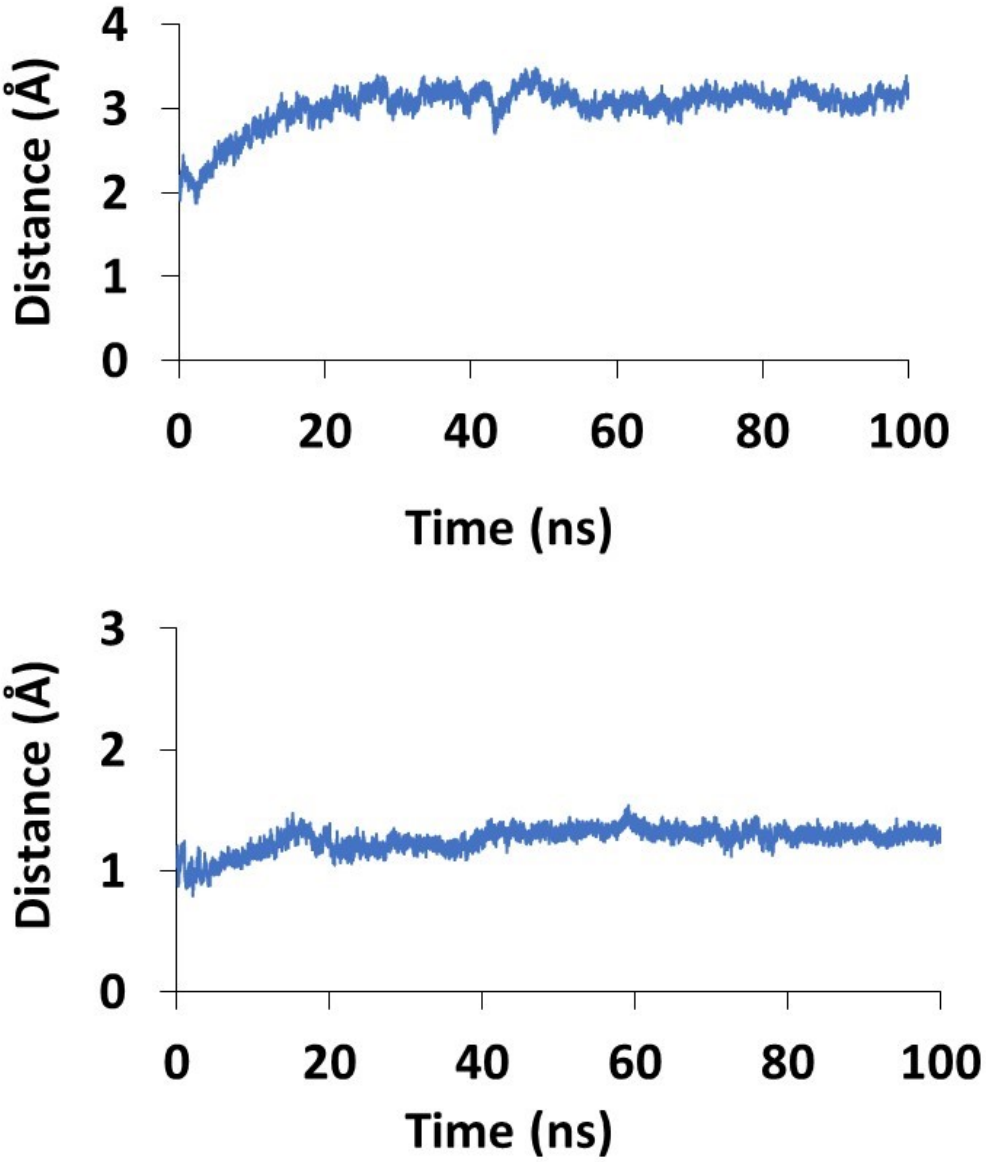

Figure S8: RMSDs of chain A (top) and insulin chain B, residues Ser9-Cys19 (bottom) of insulin fibril in which Zn^{2+} ions bind to chain B – model M5.

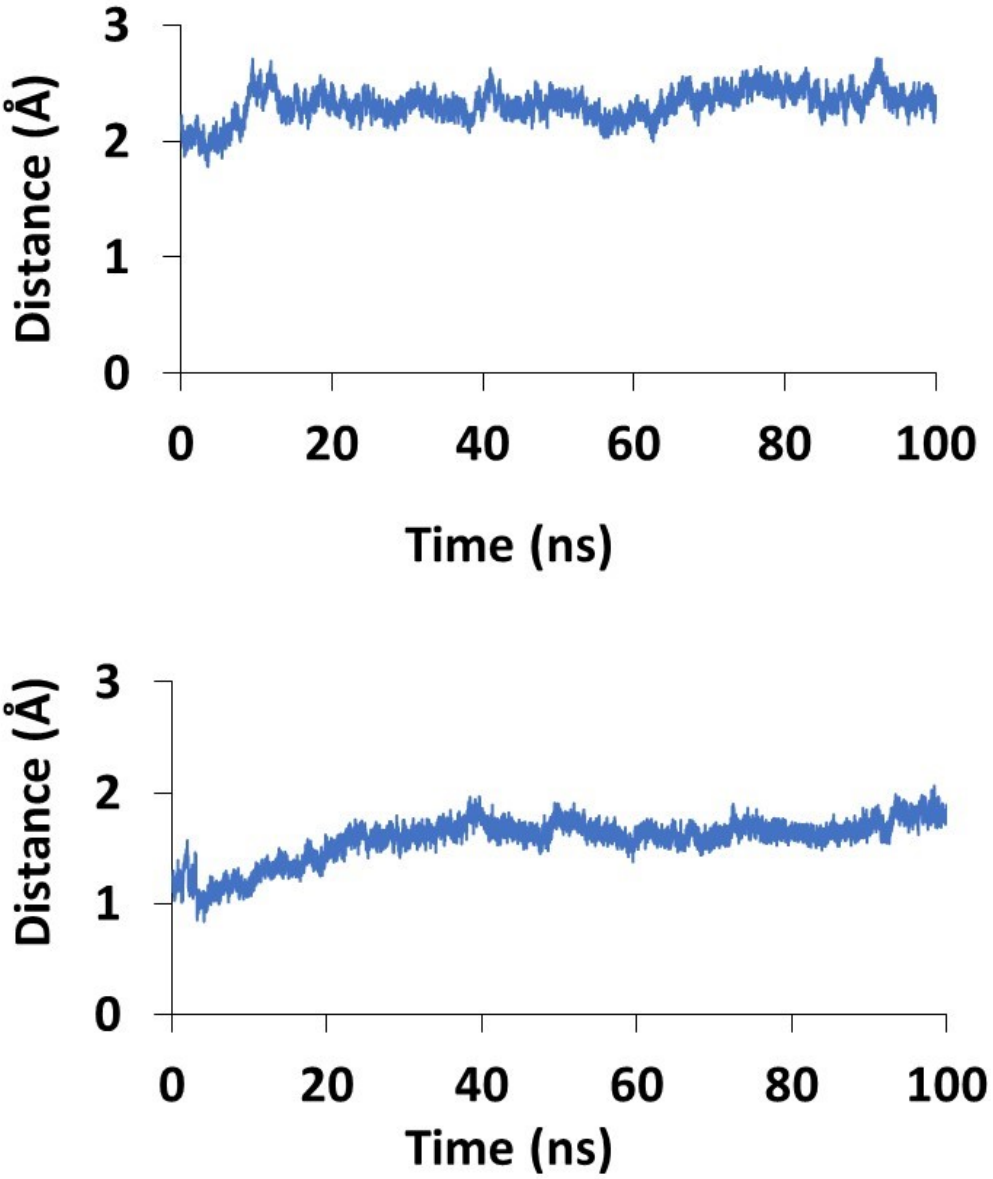

Figure S9: RMSDs of chain A (top) and insulin chain B, residues Ser9-Cys19 (bottom) of insulin fibril in which Zn^{2+} ions bind to chain B – model M6.

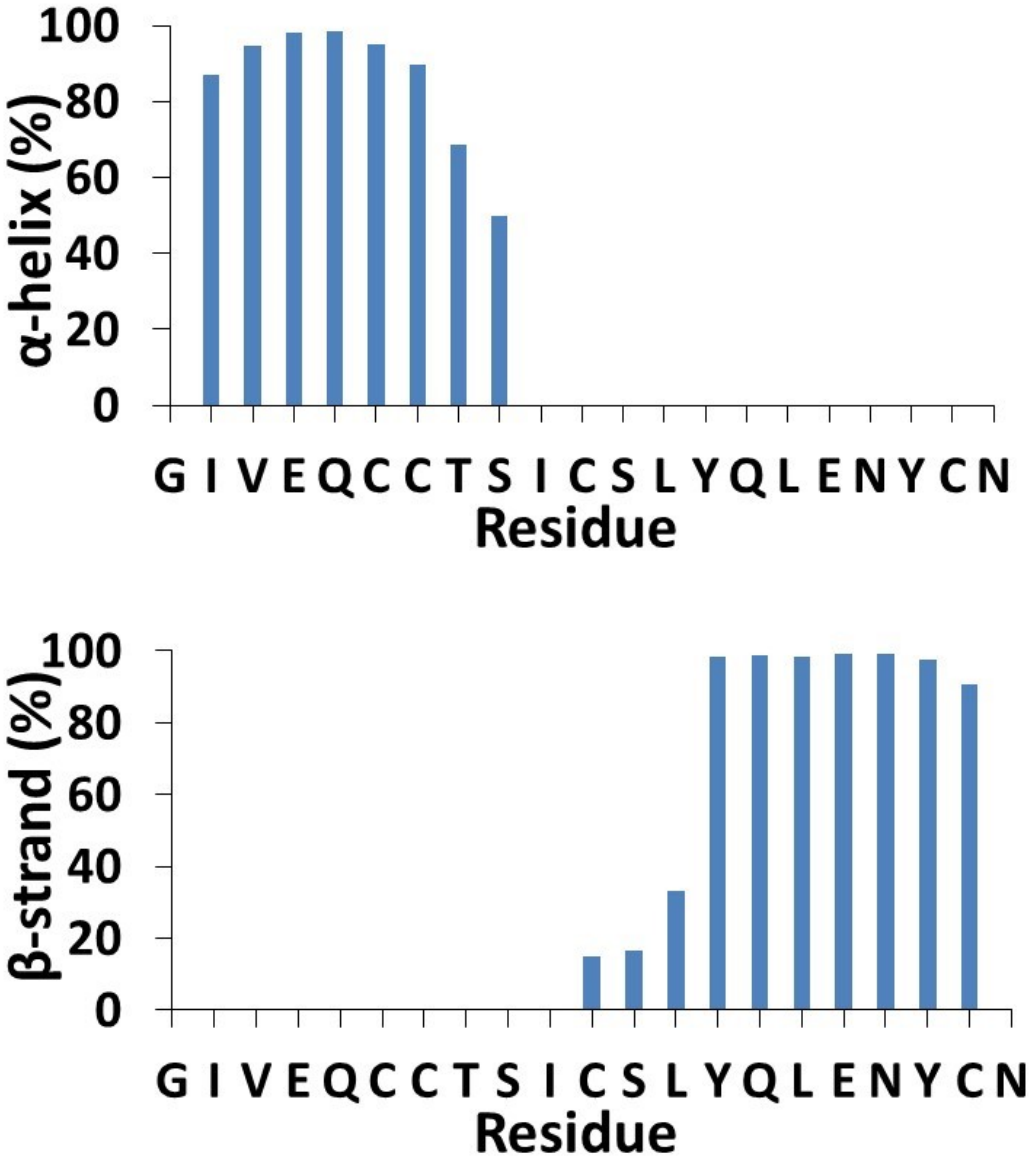

Figure S10: DSSP analysis for chain A in insulin fibril - model N, calculated from the last 5 ns of the simulations.

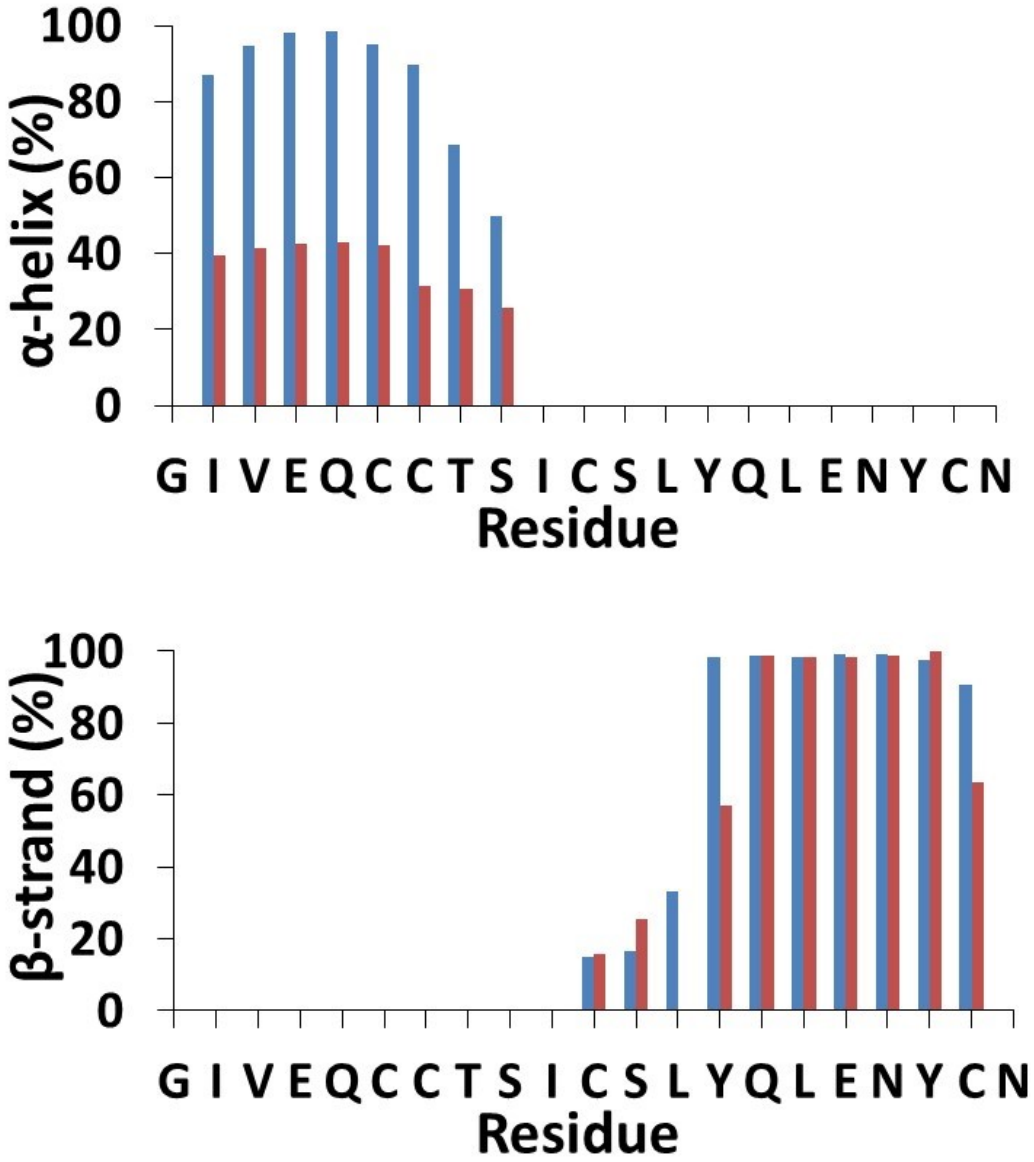

Figure S11: DSSP analysis for chain A in insulin fibrils model N (color: blue) and model M1 (color: red), calculated from the last 5 ns of the simulations.

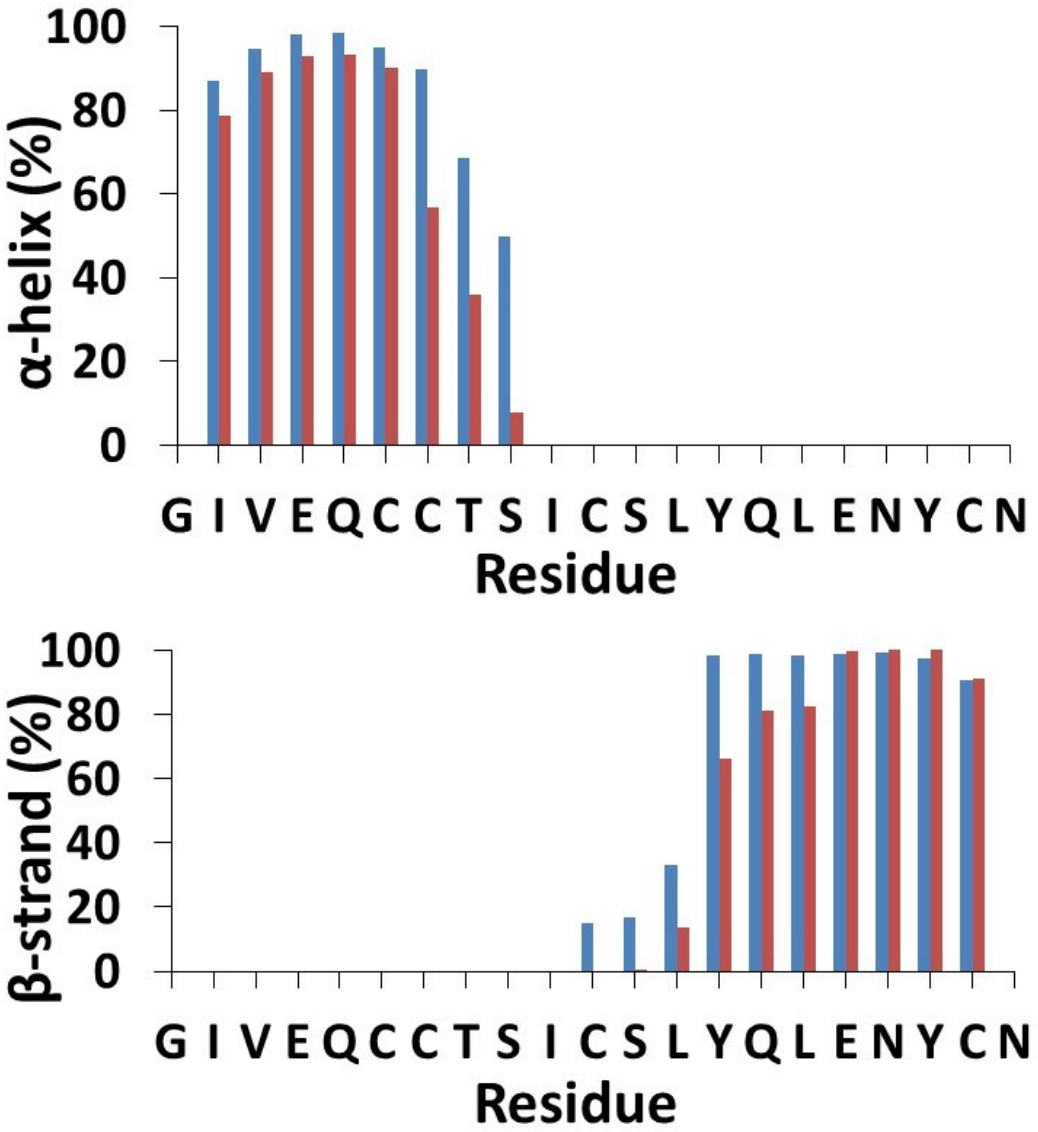

Figure S12: DSSP analysis for chain A in insulin fibrils model N (color: blue) and model M2 (color: red), calculated from the last 5 ns of the simulations.

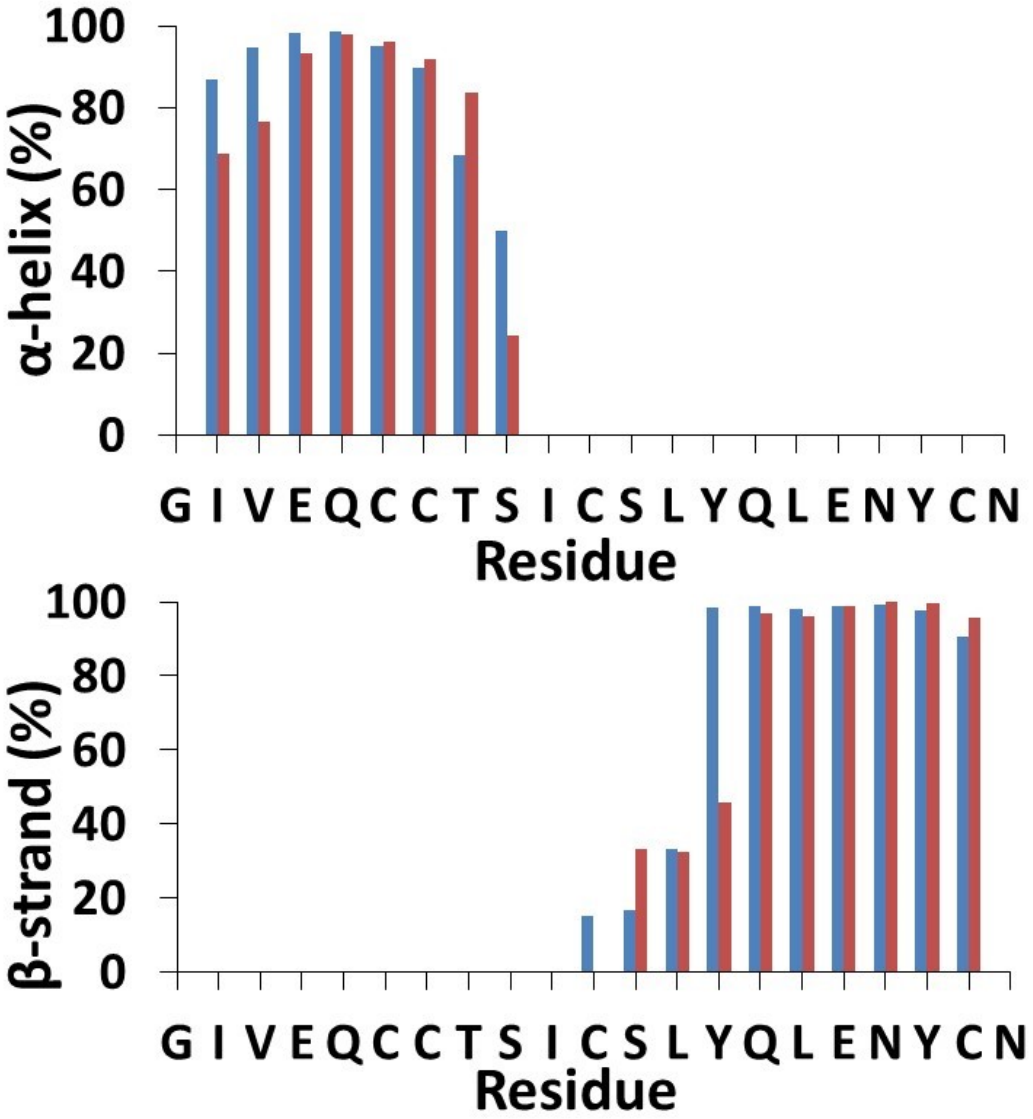

Figure S13: DSSP analysis for chain A in insulin fibrils model N (color: blue) and model M3 (color: red), calculated from the last 5 ns of the simulations.

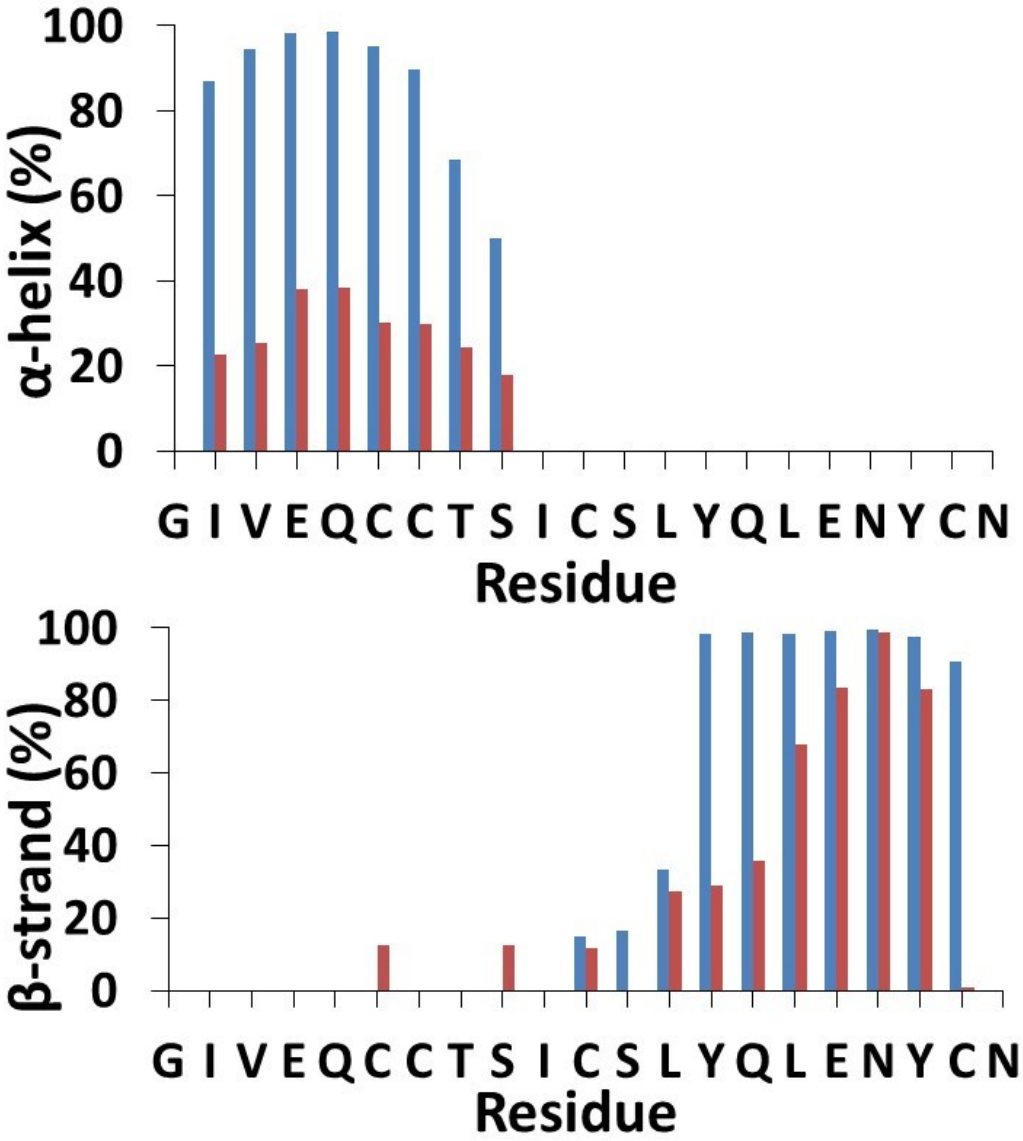

Figure S14: DSSP analysis for chain A in insulin fibrils model N (color: blue) and model M4 (color: red), calculated from the last 5 ns of the simulations.

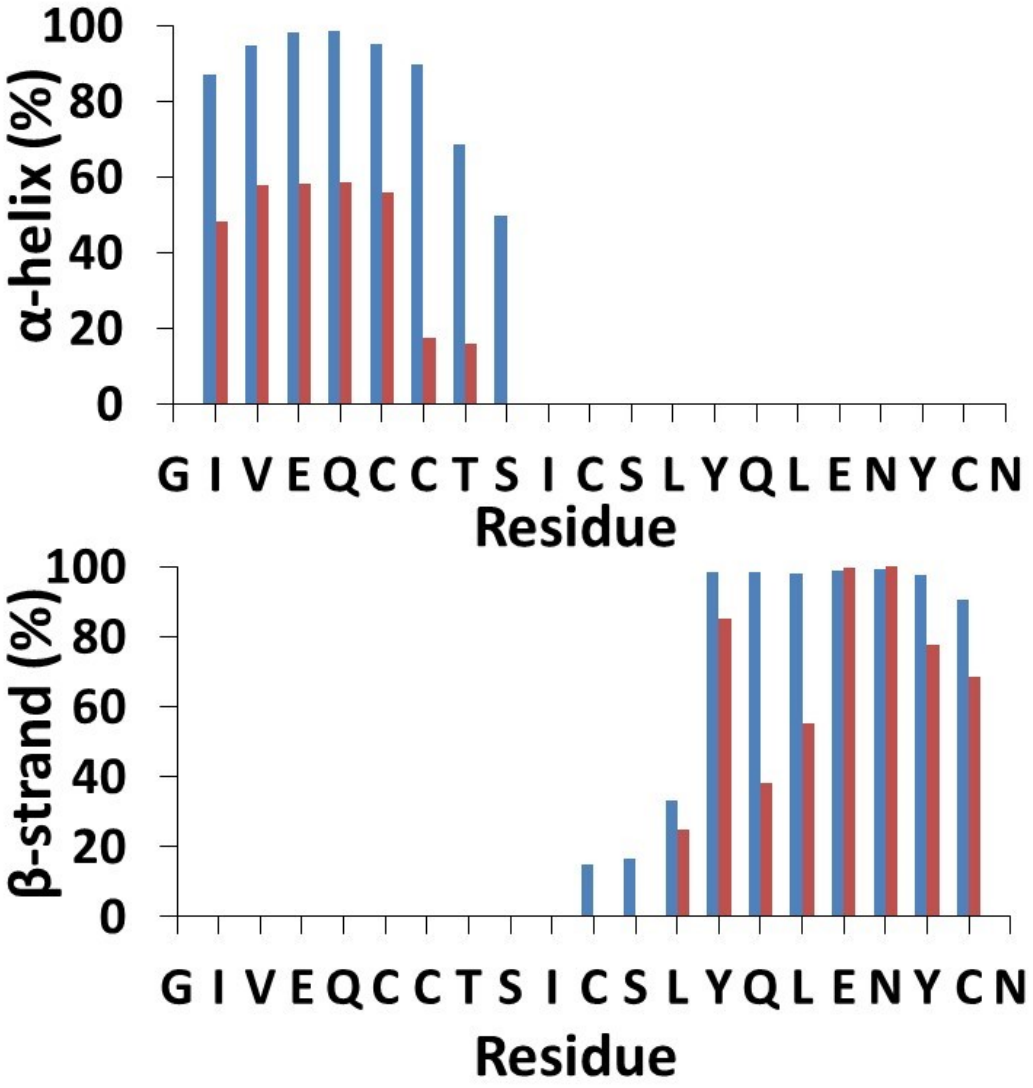

Figure S15: DSSP analysis for chain A in insulin fibrils model N (color: blue) and model M5 (color: red), calculated from the last 5 ns of the simulations.

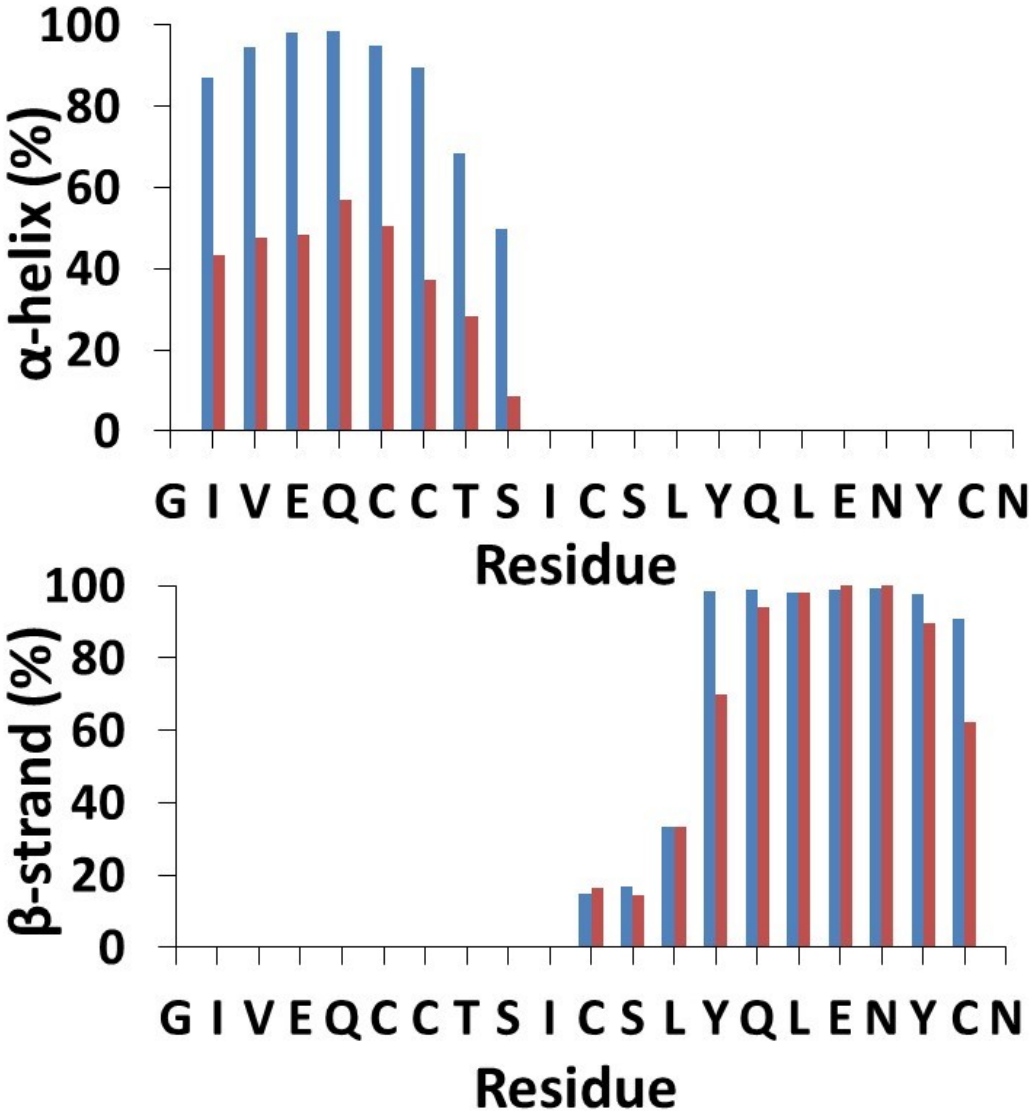

Figure S16: DSSP analysis for chain A in insulin fibrils model N (color: blue) and model M6 (color: red), calculated from the last 5 ns of the simulations.

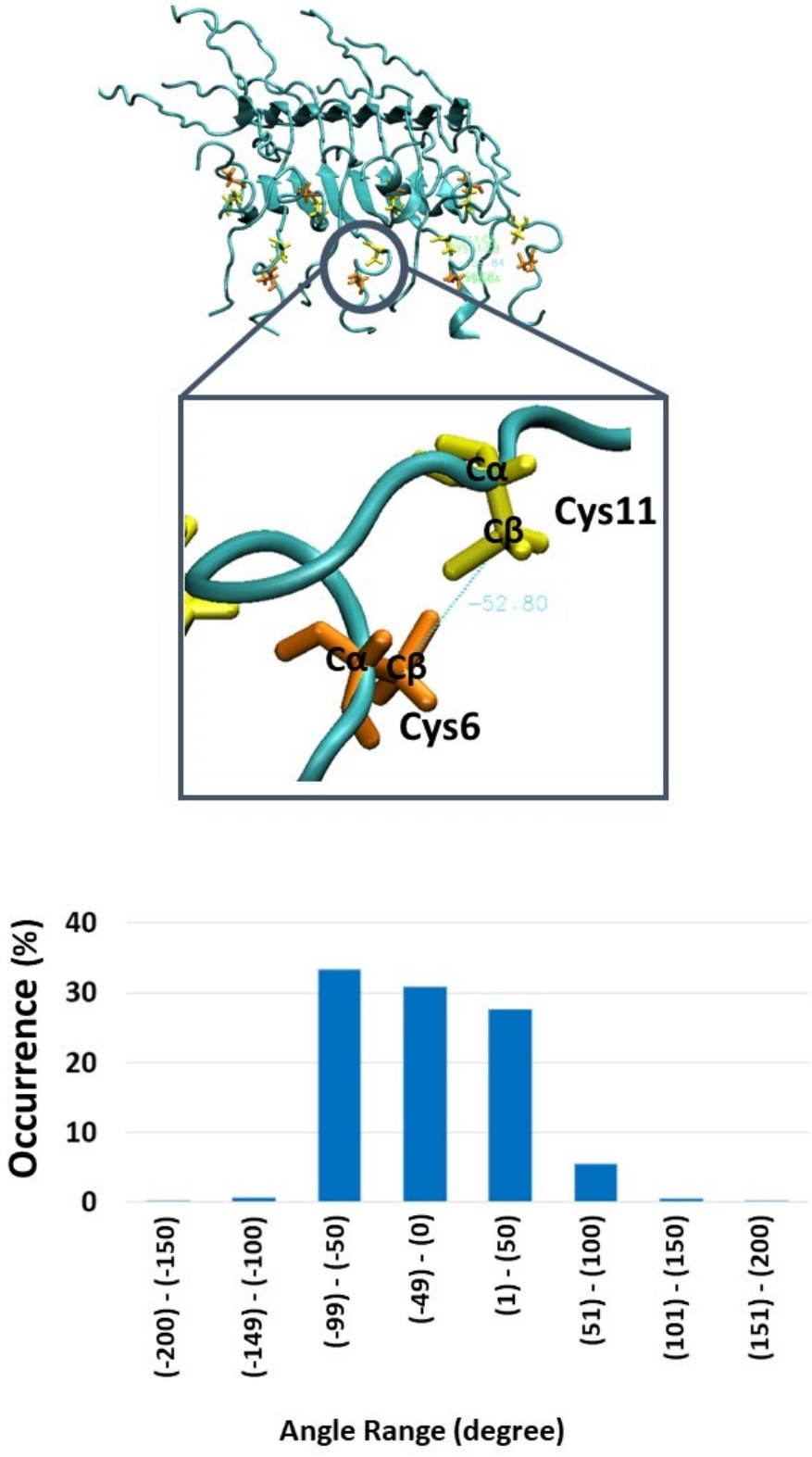

Figure S17: The dihedral angle Cα (Cys6)-Cβ(Cys6)-Cβ(Cys11)-Cα(Cys11) distribution within the intra-linkage disulfide bond in chain A for insulin in absence of Zn^{2+} ions.

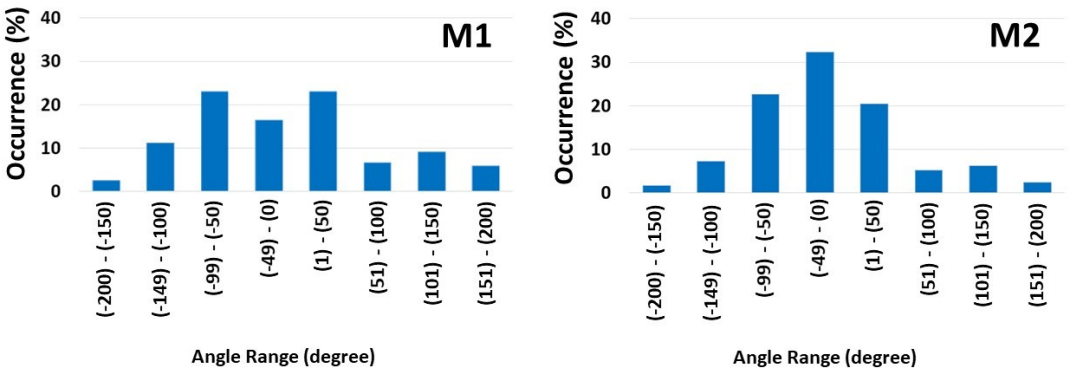

Figure S18: The dihedral angle Cα (Cys6)-Cβ(Cys6)-Cβ(Cys11)-Cα(Cys11) distribution within the intra-linkage disulfide bond in chain A for all models of insulin in presence of Zn^{2+} ions: models M1 and M2.

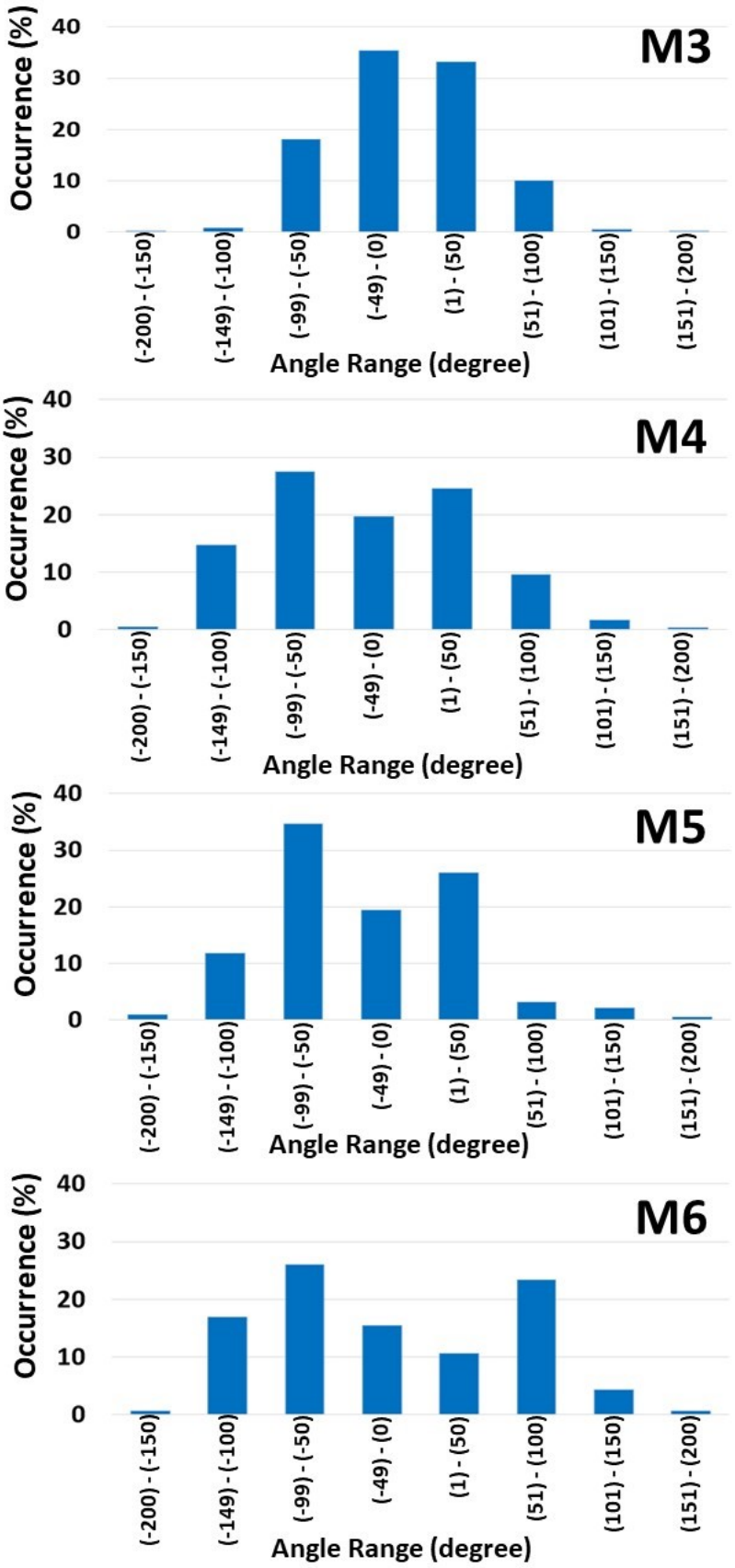

Figure S19: The dihedral angle Cα (Cys6)-Cβ(Cys6)-Cβ(Cys11)-Cα(Cys11) distribution within the intra-linkage disulfide bond in chain A for all models of insulin in presence of Zn^{2+} ions: models M3-M6.

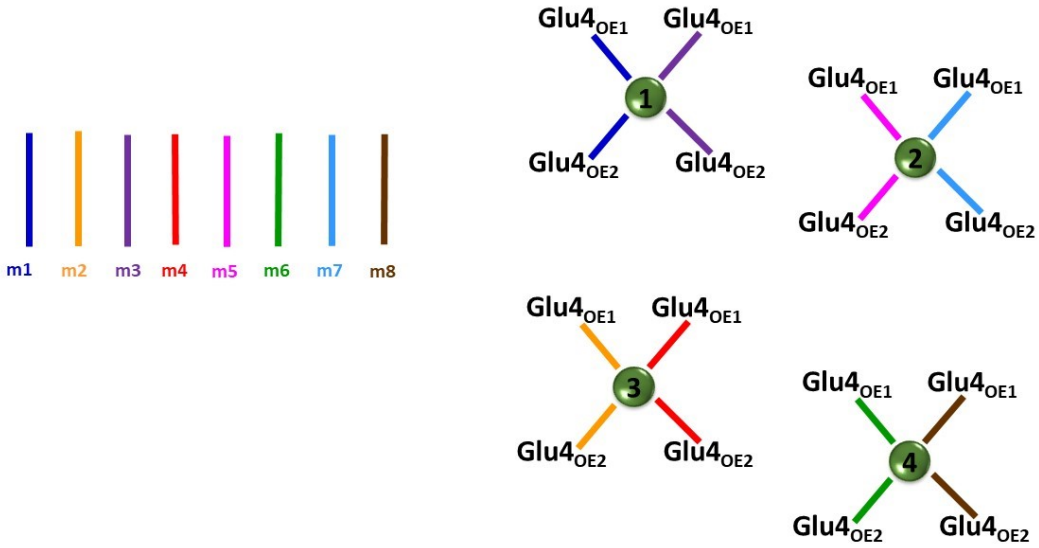

Figure S20: A scheme of the monomers within insulin fibril (left): monomer 1 (color: blue), monomer 2 (color: orange), monomer 3 (color: purple), monomer 4 (color: red), monomer 5 (color: pink), monomer 6 (color: green), monomer 7 (color: light blue), monomer 8 (color: brown). The monomers that bind each one of the four Zn^{2+} ions in model M1 (Right).

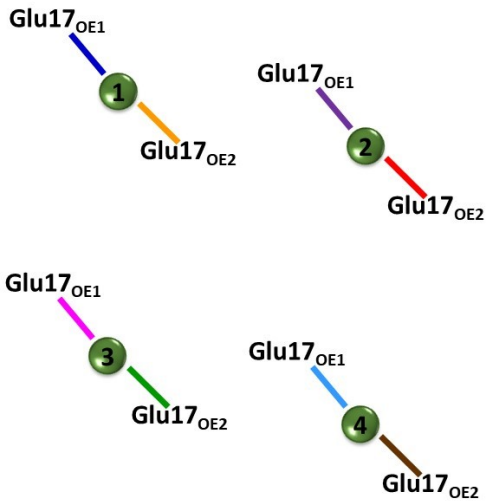

Figure S21: The monomers that bind each one of the four Zn^{2+} ions in model M2. The colors of the monomers within insulin fibril, are detailed in Figure S17.

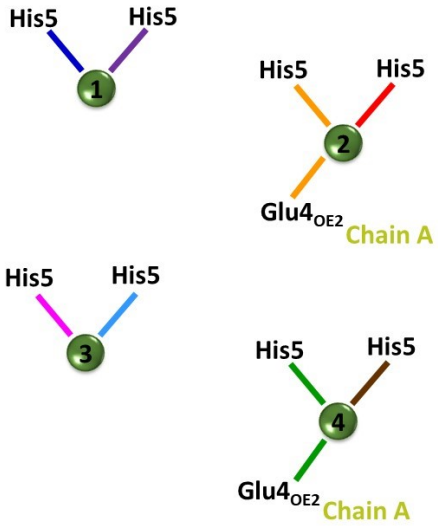

Figure S22: The monomers that bind each one of the four Zn^{2+} ions in model M3. The colors of the monomers within insulin fibril, are detailed in Figure S17.

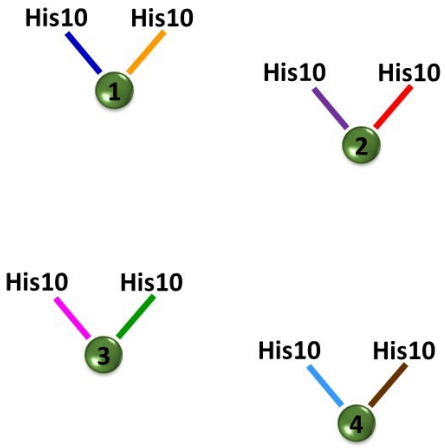

Figure S23: The monomers that bind each one of the four Zn^{2+} ions in model M4. The colors of the monomers within insulin fibril, are detailed in Figure S17.

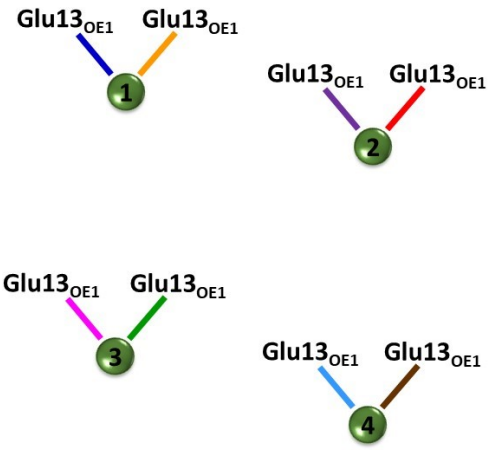

Figure S24: The monomers that bind each one of the four Zn^{2+} ions in model M5. The colors of the monomers within insulin fibril, are detailed in Figure S17.

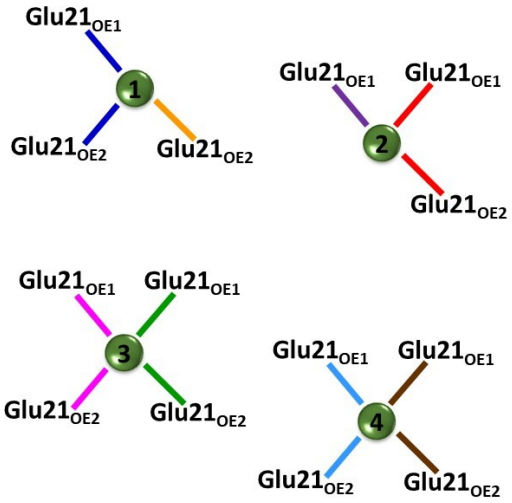

Figure S25: The monomers that bind each one of the four Zn^{2+} ions in model M6. The colors of the monomers within insulin fibril, are detailed in Figure S17.

References:

1. Lee, M. S.; Feig, M.; Salsbury, F. R.; Brooks, C. L., New analytic approximation to the standard molecular volume definition and its application to generalized born calculations. *J Comput Chem* 2003, **24**, 1348-1356.

2. Lee, M. S.; Salsbury, F. R.; Brooks, C. L., Novel generalized Born methods. *J Chem Phys* 2002, **116**, 10606-10614.

3. Hsin, K., Sheng, Y., Harding, M. M., Taylor, P., Walkinshaw, M. D., MESPEUS: a database of the geometry of metal sites in proteins. *J Appl Cryst* 2008, **41**, 963-968.

4. Miller, Y.; Ma, B.; Nussinov, R., Zinc ions promote Alzheimer Abeta aggregation via population shift of polymorphic states. *Proc Natl Acad Sci U S A* 2010, **107**, 9490-5.

5. Bloch, D. N.; Kolkowska, P.; Tessari, I.; Baratto, M. C.; Sinicropi, A.; Bubacco, L.; Mangani, S.; Pozzi, C.; Valensin, D.; Miller, Y., Fibrils of alpha-Synuclein Abolish the Affinity of Cu(2+)-Binding Site to His50 and Induce Hopping of Cu(2+) Ions in the Termini. *Inorg Chem* 2019, **58**, 10920-10927.

6. Ben-Shushan, S.; Hecel, A.; Rowinska-Zyrek, M.; Kozlowski, H.; Miller, Y., Zinc Binding Sites Conserved in Short Neuropeptides Containing a Diphenylalanine Motif. *Inorg Chem* 2020, 59, 925-929.

7. Ben-Shushan, S.; Miller, Y., Neuropeptides: Roles and Activities as Metal Chelators in Neurodegenerative Diseases. *J Phys Chem B* 2021, **125**, 2796-2811.

8. Ben-Shushan, S.; Miller, Y., Molecular Mechanisms and Aspects on the Role of Neuropeptide Y as a Zn(2+) and Cu(2+) Chelator. *Inorg Chem* 2021, **60**, 484-493.